Thermodynamic and Kinetic Studies on Alkoxylation of Camphene over Cation Exchange Resin Catalysts

Huiqin Nie, Ruyin Xu, Feng Zhang, Zheng Zhou, and Zhibing Zhang
Separation Engineering Research Center of Nanjing University, Key Laboratory of Mesoscopic Chemistry of Ministry of Education of China, School of Chemistry and Chemical Engineering, Nanjing University, Nanjing 210093, P.R. China

Gaodong Yang
Research and Development Department, Nanjing Eneteks Company Limited, Nanjing 210018, P.R. China

DOI 10.1002/aic.14786
Published online March 25, 2015 in Wiley Online Library (wileyonlinelibrary.com)

The alkoxylation of camphene with 2-methyl-1,3-propanediol was studied using anhydrous macroporous and strong acid cation exchange resins as catalysts. The effects of various parameters, such as catalyst type, solvent, molar ratio of reactants, reaction temperature, and reusability of catalysts, were investigated in a 250 mL stirred tank reactor to optimize the reaction conditions. The UNIFAC group contribution method was used to correct liquid nonideality, giving the thermodynamic equilibrium constant at 333–370 K. The enthalpy changes calculated by three different methods (Gaussian 03, constant, and a function of temperature) were compared. The value (-74.6 ± 3.3 kJ/mol) calculated by the last method was closer to the theoretical value (-75.73 kJ/mol) than that given by the second method (-30.2 ± 1.2 kJ/mol). A Langmuir–Hinshelwood–Hougen–Watson model based on activity was used to fit experimental data and the activation energy was 29.14 kJ/mol. The optimized reaction conditions were also verified in a 5 L reaction kettle. © 2015 American Institute of Chemical Engineers *AIChE J*, 61: 1925–1932, 2015
Keywords: alkoxylation, camphene, cation exchange resin, kinetics, thermodynamics

Introduction

Monoterpenes are important renewable substrates widely used in the flavor, fragrance, and pharmaceutical industries.[1–4] Acid-catalyzed alkoxylation of monoterpenes is one of the crucial synthetic routes that produce valuable monoterpenic ethers as flavors and fragrances in perfume and cosmetic products, or as additives in medicine and agricultural chemicals.[5,6] Therefore, it is of great industrial significance to study the alkoxylation of monoterpenes.

Up to now, monoterpenes have been alkoxylated with different kinds of catalysts. Royals[7] synthesized terpinyl ethers from *d*-limonene in the presence of sulfur acid, which led to a serious corrosion problem. Organic sulfuric acids have also been used in the alkoxylation of monoterpenes. For instance, Lin and Gu[8] studied the reaction of camphene with ethanol using *p*-toluenesulfonic acid as the catalyst under microwave irradiation. However, the liquid acid also caused severe environmental pollution.

The deficiencies caused by liquid catalysts can be remedied by solid acid ones. Pito et al.[9] discussed the methoxylation of α-pinene using heteropolyacids immobilized on silica as catalysts at 60°C, mainly yielding α-terpinyl methyl ether. However, bornyl methyl ether, fenchyl methyl ether, and some isomerization products were also generated as byproducts. Caiado et al.[10] compared the alkoxylating activities of different linear and branched alcohols against camphene in the presence of silica-occluded tungstophosphoric acid (4.2% w/w) at 60–80°C. Hensen et al.[11] alkoxylated limonene and α-pinene with C_1-C_5 alcohols over *β*-zeolite. Limonene and α-pinene were well alkoxylated with linear alcohols, but the selectivity for corresponding ethers sharply decreased when branched alcohols were used.

Among the catalysts currently available, the noncorrosive, recyclable cation exchange resins are popular due to high catalytic activity and facile separation based on several industrial processes such as olefin hydration,[12–14] esterification,[15–19] phenols alkylation,[20] ester hydrolysis,[21,22] isomerization, and acetaldehyde acetalization.[23–26]

The design of reactors is determined by equilibrium constant, reaction enthalpy change, and reaction rate equation. The thermodynamics and kinetics of alkoxylation of camphene have rarely been studied. Caiado et al.[10] studied the reaction kinetics of camphene with low-molecular-weight alcohol in the presence of silica-occluded $H_3PW_{12}O_{40}$. They assumed the alcohol concentration remained constant and the reaction was irreversible, and the reaction order with respect to camphene was 0.68. Radbil' et al.[27] obtained the kinetic data of camphene alkoxylation in the presence of heteropoly acid and H_2SO_4 with excess alcohol. They also calculated the equilibrium concentration constants without considering the nonideality of solution.

Correspondence concerning this article should be addressed to Z. Zhang at zbzhang@nju.edu.cn or Z. Zhou at zhouzheng1973@gmail.com.

Table 1. Properties of Different Cation Exchange Resins

Properties	Lewatit 2620	CT 482
Physical form	Opaque beads	Opaque beads
Ionic form as shipped	Hydrogen	Hydrogen
Concentration of active sites[a]	5.10 eq/kg	2.75 eq/kg
Particle size range	0.5–0.62 mm	0.425–1.25 mm
Surface area	14.3 m^2/g	9.0 m^2/g
Temperature stability	413 K	463 K
Manufacturer	Lanxess Chemical Co., PRC	Purolite Co., PRC

[a]Measured by titration method.

In this study, camphene was alkoxylated with 2-methyl-1,3-propanediol (MPO) into isobornyl hydroxyl isobutyl ether (IHIE) using anhydrous Lewatit2620. IHIE is valuably applicable owing to long-lasting, woody, dry amber, and cedar scents. The reaction conditions were optimized in a 250-mL stirred tank reactor. Thermodynamic parameters, such as the equilibrium constant at 333–370 K and reaction enthalpy change, were also calculated and compared to the theoretical ones computed by Gaussian 03. Kinetics of the alkoxylation of camphene with MPO catalyzed by Lewatit2620 was described by Langmuir–Hinshelwood–Hougen–Watson (LHHW) model. A scale-up experiment was carried out in a 5 L double layer glass reaction kettle, which laid a good foundation for industrialization.

Experimental Section

Materials

Industrial grade products of camphene (including camphene and tricyclene, content $\geq 93\%$) were obtained from Xiamen Doingcom Chemical Company (China). MPO (purity $\geq 99\%$) was purchased from Aladdin Chemistry Co., (China). Analytical grade 1,4-dioxane was procured from Nanjing Chemical Reagent Co., (China). All chemicals were used without further purification.

Two kinds of strong acid cation exchange resins (Lewatit2620, CT482) were used as catalysts. Their properties are listed in Table 1. These catalysts were washed several times with distilled water to eliminate free acids and dried at 363 K to remove moisture completely.

Apparatus and procedures

The reactions were performed in a 250-mL glass stirred tank reactor equipped with an online device measuring the agitation speed. A condenser opening to the atmosphere was housed on the reactor with a thermometer to measure the reaction temperature. To maintain the required reaction temperature, the reactor was immersed in a constant-temperature water bath. Reactants were fed at the desired molar ratio with agitation. When the temperature achieved the desired value, the catalysts were charged into the reactor and the reaction began. Samples were taken out at appropriate time intervals, diluted with 1,4-dioxane, and then analyzed by gas chromatography (GC).

Analysis

All samples were analyzed by a gas chromatograph (Shimadzu, model GC-2014C) equipped with a methyl polysiloxane capillary column (HP-5, 30 m $\times$ 0.32 mm $\times$ 0.25 μm). Nitrogen was used as the carrier gas at the flow rate of 3 mL/min. The injection port temperature and detector temperature were set at 573 and 553 K, respectively. The column temperature was first held at 343 K for 1 min, increased to 373 K at the rate of 5 K/min, held for another 1 min, and finally increased to 523 K at the rate of 20 K/min for 3 min. The injection volume was 0.2 μL. A GC-TOF gas chromatography mass spectrometry was used to identify the main product.

Results and Discussion

The reaction of camphene alkoxylation is shown in Figure 1. Carbenium ion (2), which first forms under the catalysis of acid, is converted into nonclassical carbenium ion (3) through Wagner–Meerwein rearrangement.[28,29] Afterward, MPO nucleophilically attacks the nonclassical carbenium ion (3) to generate IHIE (4) and bornyl hydroxyl isobutyl ether (5), with the latter being scarce due to steric effect.

Process variables investigation

Effect of Catalyst Type. Two different types of cation exchange resins were used in the alkoxylation of camphene. The reaction was accelerated with Lewatit2620 compared

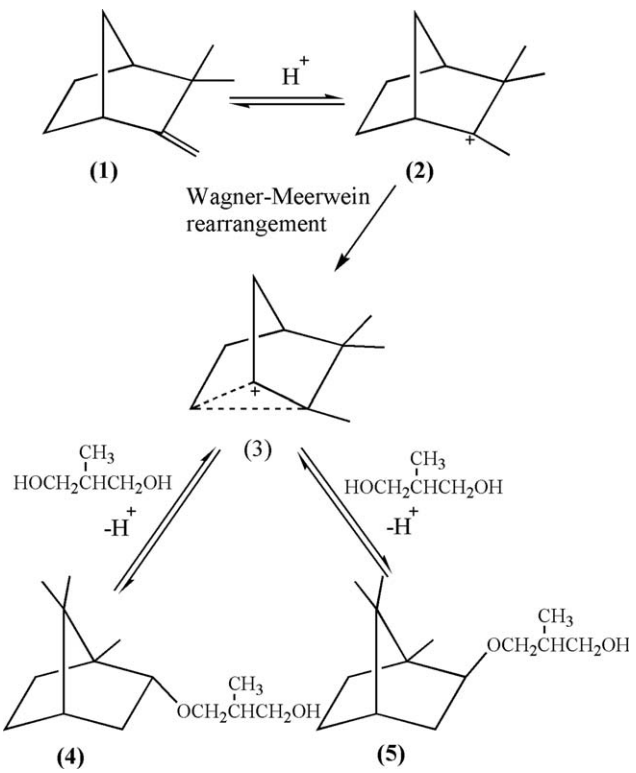

Figure 1. Reaction for the alkoxylation of camphene: (1) camphene; (2) carbenium ion; (3) nonclassical carbenium ion; (4) IHIE; (5) bornyl hydroxyl isobutyl ether.

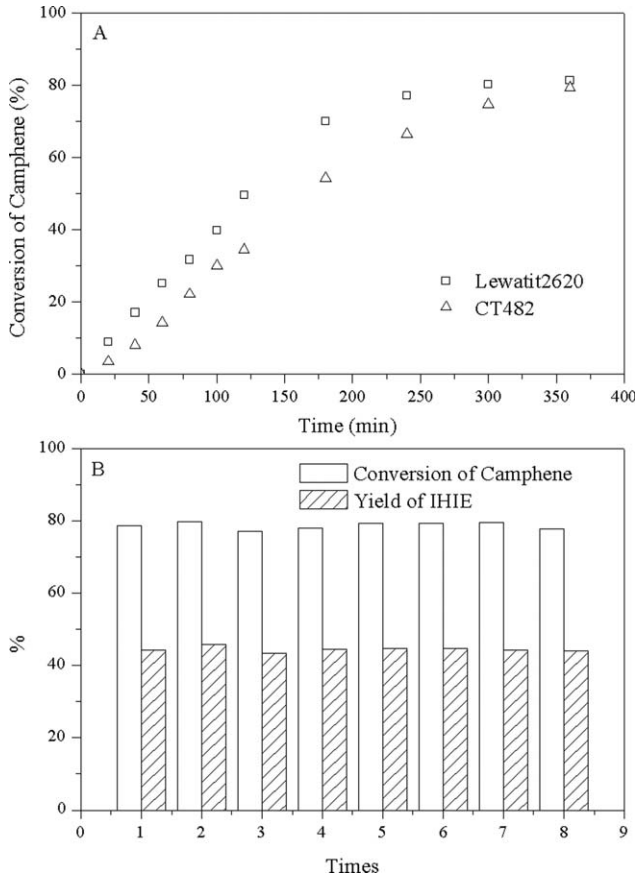

Figure 2. (A) Effect of catalyst type on the conversion of camphene (temperature: 353 K; catalyst loading: 20% (w/w); molar ratio of camphene: MPO was 1:1, average particle size: 0.5–0.62 mm); (B) results of the reusability of catalysts (temperature: 353 K; Lewatit2620 as catalyst; catalyst loading: 20% (w/w); molar ratio of camphene: MPO was 1:1, average particle size: 0.5–0.62 mm, 4h).

with that with CT482 (Figure 2A) owing to the higher concentration of active sites.

The reusability of catalyst is another significant factor for industrial application. In this study, the catalysts were separated from the reaction mixture by filtration, washed with distilled water, and dried at 363 K for reuse. Both the conversion of camphene and the yield of IHIE almost remained the same after Lewatit2620 was reused eight times (Figure 2B), indicating that this catalyst is highly reusable and potentially industrially applicable. Accordingly, anhydrous Lewatit2620 was chosen as the catalyst thereafter.

Effect of Solvent. Camphene is slightly soluble in alcohol and is solid at room temperature and pressure due to low melting point (50°C). Therefore, solvent is introduced to increase the mutual solubility of reactants. Low-molecular-weight alcohols, such as methanol, are ineligible because of high activity. Common organic solvents, such as cyclohexane, *n*-hexane, THF, benzene, carbon tetrachloride, chloroform, carbon dichloride and DMF, cannot dissolve them both simultaneously. The two reactants are soluble in 1,4-dioxane. However, solvent only managed to speed up the reaction before 180 min and failed to do so thereafter (Figure 3). Probably, the increased mutual solubility of two reactants eliminated the influence of internal diffusion and elevated the reaction rate, while the shifting of equilibrium was caused by the decrease of ion exchange capacity owing to the complexation of sulfonate groups in nonaqueous solvent.[30] To reduce the separation cost, camphene was alkoxylated without any solvents.

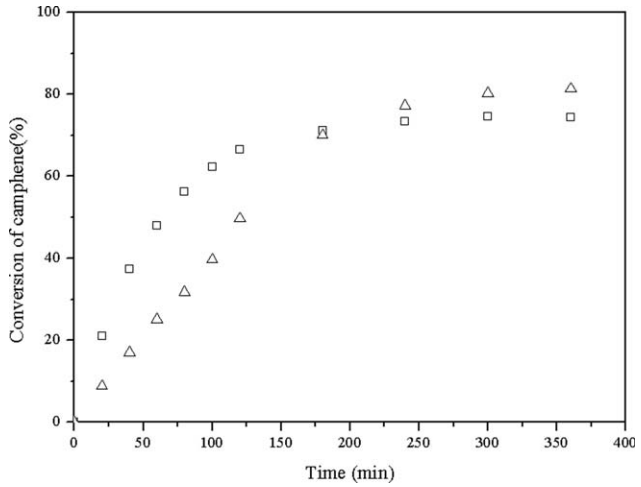

Figure 3. Effect of solvent on the conversion of camphene (temperature: 353 K; Lewatit2620 as catalyst; catalyst loading: 20% (w/w); molar ratio of camphene: MPO was 1:1, average particle size: 0.5–0.62 mm) (□) 1, 4-dioxane (the amount is equivalent to the total mass of camphene and MPO); (△) no solvent.

Effect of Initial Molar Ratio of Reactants. Experiments with initial molar ratios of camphene to MPO from 1:0.5 to 1:3 were carried out with catalyst loading of 20% at 353 K. As shown in Figure 4, when camphene/MPO ratio is in the range of 1:0.75–1:2, as the amount of MPO increases, the conversion of camphene rises. When the molar ratio is 1:0.5, the reaction rate is faster than that of 1:0.75. This can be ascribed to mechanism transformation from the carbonium

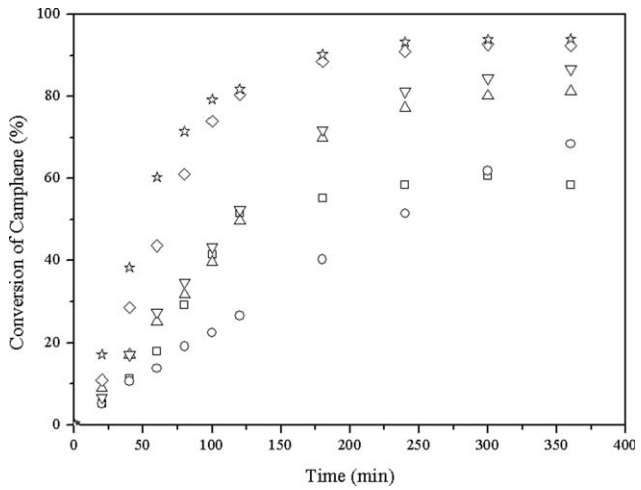

Figure 4. Effect of initial molar ratio of reactants on the alkoxylation of camphene (temperature: 353 K; Lewatit2620 as catalyst; catalyst loading: 20% (w/w, average particle size: 0.5–0.62 mm). (□) 1:0.5; (○) 1:0.75; (△) 1:1; (▽) 1:1.25; (◇) 1:2; (☆) 1:3.

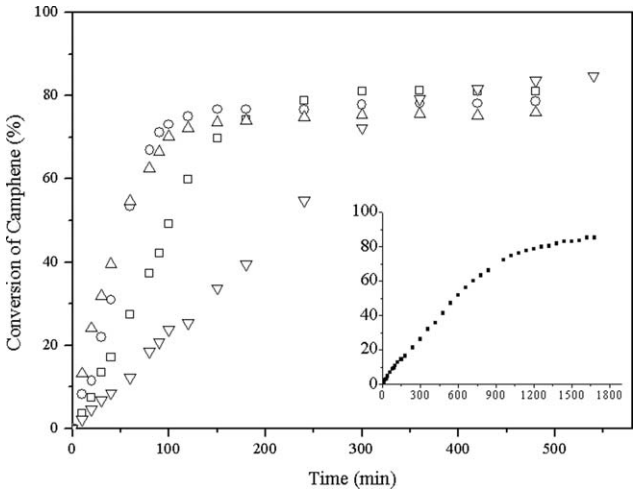

Figure 5. Effect of temperature on the alkoxylation of camphene (Lewatit2620 as catalyst; catalyst loading: 20% (w/w); molar ratio of camphene: MPO was 1:1, average particle size: 0.5–0.62 mm) (■) 333 K; (▽) 343 K; (□) 353 K; (○) 363 K; (△) 370 K.

ion mechanism to a concerted reaction on the associated network of sulfonic groups.[31,32] As MPO is much more expensive than camphene, the initial molar ratio of MPO to camphene was selected at 1:1 herein to maximize the overall economic profit.

Effect of Temperature. The effects of temperature on the conversion of camphene and the yield of IHIE were investigated from 333 to 370 K. The conversion of camphene was elevated as temperature increased from 333 to 353 K, and was then reduced as the temperature kept rising (Figure 5), because higher temperature accelerated the reaction and shifted the equilibrium of this exothermic reaction backward. Moreover, higher temperature brought more byproducts (α-terpinyl ether, γ-terpinyl ether, etc.) caused by impurities and thus lowered the selectivity.

Thermodynamic study

Chemical Equilibrium. The equilibrium state was assessed by checking the constancy of the conversion of camphene. Experiments at different temperatures lasted long enough for the reaction to reach equilibrium. Equilibrium constant can be obtained from the experimental data at different temperatures. The activity-based equilibrium constant K is defined as Eq. 1[33]

$$K=\prod a_i^{\nu_i}=\frac{a_{\mathrm{IHIE}}}{a_{\mathrm{cam}}a_{\mathrm{MPO}}}=\left(\frac{x_{\mathrm{IHIE}}}{x_{\mathrm{cam}}x_{\mathrm{MPO}}}\right)\left(\frac{\gamma_{\mathrm{IHIE}}}{\gamma_{\mathrm{cam}}\gamma_{\mathrm{MPO}}}\right)=K_xK_\gamma \tag{1}$$

where a_i ($= x_i\gamma_i$) denotes the activity of component i in the bulk liquid phase, x_i is the mole fraction of component i, and γ_i is the activity coefficient of component i. The UNIFAC group contribution method was used to determine the activity coefficients based on the volume and area parameters of the groups and their interaction parameters reported previously.[34]

The calculated equilibrium constants at different temperatures are presented in Table 2. As the equilibrium constants decreased with increasing temperature, the reaction was exothermic. Conversely, K_γ was significantly different from unity, so the nonideality of the mixture should also be taken into account in calculation.

Table 2. Calculated Equilibrium Constants for Alkoxylation of Camphene

T (K)[a]	K_x	K_γ	K
333	53.6 ± 3.6	0.150 ± 0.001	8.04 ± 0.59
343	39.7 ± 2.6	0.153 ± 0.001	6.06 ± 0.43
353	27.4 ± 1.5	0.157 ± 0.002	4.29 ± 0.29
363	21.5 ± 1.1	0.160 ± 0.001	3.44 ± 0.19
370	16.3 ± 0.8	0.163 ± 0.001	2.66 ± 0.14

[a]$T \pm 0.2$ K.

Assuming that the reaction enthalpy is constant at the operating temperatures, reaction enthalpy (Δ_rH^0) and entropy (Δ_rS^0) changes can be calculated from the equation below

$$\ln \mathrm{K}=-\frac{\Delta_rG^0}{RT}=-\frac{\Delta_rH^0}{RT}+\frac{\Delta_rS^0}{R} \tag{2}$$

By fitting the experimental values of equilibrium constants at various temperatures to Eq. 2 (Figure 6A), the enthalpy (Δ_rH^0) and entropy (Δ_rS^0) changes of the reaction can be obtained from the slope and the intercept, respectively. The temperature dependence of equilibrium is presented as Eq. 3 with R^2 of 0.995. The reaction enthalpy change, entropy change, and Gibbs free-energy are listed in Table 3

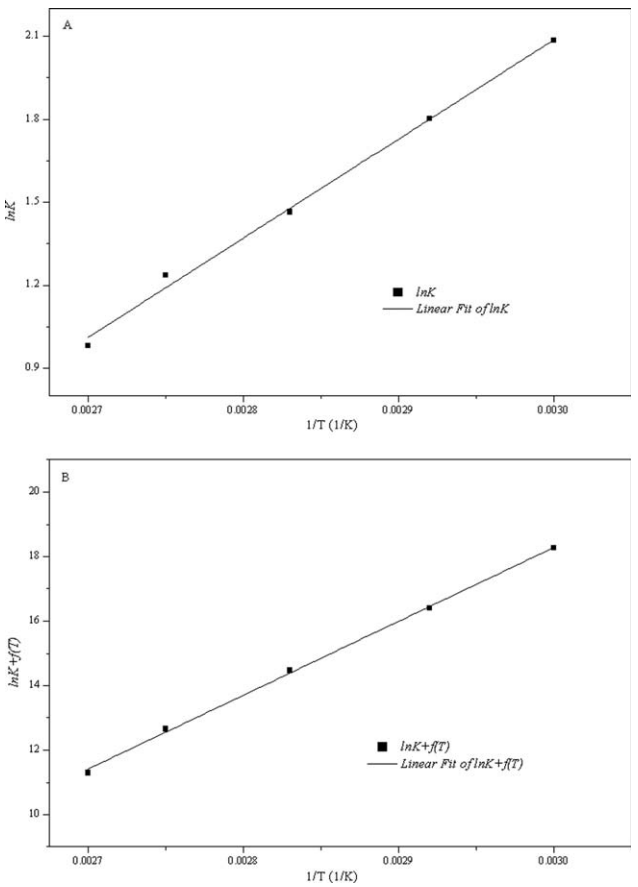

Figure 6. Comparison of values obtained experimentally and those predicted from linear model. (A) ln$K$ vs. 1/T; (B) [ln$K$ + $f(T)$] vs. 1/T.

Table 3. Enthalpy, Entropy, and Gibbs Free Energy Changes of Camphene Alkoxylation at 298 K

	$\Delta_r H^0$ (kJ/mol)	$\Delta_r S^0$ (J/mol K)	$\Delta_r G^0$ (kJ/mol)
$\Delta_r H^0$ constant	-30.2 ± 1.2	-73.4 ± 3.4	-8.38 ± 2.2
$\Delta_r H^0$ as $f(T)$	-74.6 ± 3.3	-210.9 ± 9.4	-11.8 ± 6.1
Gaussian Calculation	-75.73	-181.59	-21.59

$$\ln K = \frac{3636.7 \pm 142.6}{T} - (8.8 \pm 0.4) \tag{3}$$

However, the enthalpy actually changes significantly over the temperature range. Its dependence on temperature can be calculated by the Kirchhoff equation (Eq. 4)

$$\frac{d\Delta_r H}{dT} = \sum_i v_i C_{p,i} \tag{4}$$

By combining the Kirchhoff and the Vant' Hoff equations (Eq. 5), the entropy, and Gibbs energy changes and ln$K$ as a function of temperature are given as Eqs. 6–9

$$\frac{d\ln K}{dT} = \frac{\Delta_r H}{RT^2} \tag{5}$$

$$\Delta_r H = I_K + aT + \frac{b}{2}T^2 + \frac{c}{3}T^3 + \frac{d}{4}T^4 \tag{6}$$

$$\Delta_r S = R \cdot I_H + a(\ln T + 1) + bT + \frac{c}{2}T^2 + \frac{d}{3}T^3 \tag{7}$$

$$\Delta_r G = I_K - R \cdot I_H \cdot T - aT\ln T - \frac{b}{2}T^2 - \frac{c}{6}T^3 - \frac{d}{12}T^4 \tag{8}$$

$$\ln K = I_H - \frac{I_K}{RT} + \frac{a}{R}\ln T + \frac{b}{2R}T + \frac{c}{6R}T^2 + \frac{d}{12R}T^3 \tag{9}$$

$$C_{p,i} = a_i + b_i T + c_i T^2 + d_i T^3 \tag{10}$$

$$a = \sum_i v_i a_i; b = \sum_i v_i b_i; c = \sum_i v_i c_i; d = \sum_i v_i d_i$$

where v_i is the reaction stoichiometric coefficient, $C_{p,i}$ is the molar heat capacity of component i, and a_i, b_i, c_i, and d_i are estimated by the Rowlinson–Bondi method[34,35] and fitted to a third-order equation (Table 4). I_H and I_K can be gained by the slope and the intercept of the linear dependence of $[\ln K + f(T)]$ vs. $1/T$ (Figure 6B), respectively. The following equation is then derived by linear regression

$$\ln K + f(T) = \frac{23192.0 \pm 398.7}{T} - (51.3 \pm 1.1) \tag{11}$$

For convenience of comparison, the enthalpy and entropy changes of the reaction are calculated from Gaussian calculation method. All the geometries were fully optimized with a Gaussian 03 program by the DFT-based RB3LYP method.

The enthalpy, entropy, and free energy changes calculated by the three methods are summarized in Table 3. When $\Delta_r H^0$ was assumed to be constant, the enthalpy, entropy, and free energy changes were significantly different from those calculated by Gaussian 03 (differences: 60.1, 59.6, and 61.2%, respectively). However, they changed following the same trend. In contrast, the computed enthalpy change was, by considering $\Delta_r H^0$ as a function of temperature, close to the theoretical data (difference: 1.4%). Therefore, $\Delta_r H^0$ cannot be treated as constant in reactor design. In the meantime, the difference between entropy changes was 16.2%, which was significantly lower than that (45.4%) obtained without considering the influence of temperature. Hence, the dependence of entropy change on temperature cannot be neglected in practice. The differences in entropy, which can be ascribed to the uncertainty (fluctuations of atmospheric pressure and temperature, etc.) in chemical analysis, led to significantly different free energy changes. In addition, as Gaussian calculation was performed in an ideal state, the difference between theoretical and experimental values was inevitable.

Table 4. Thermochemical Data of Camphene, MPO, and IHIE

Property	Camphene	MPO	IHIE
a_i (J/mol·K)	-134.0295	24.9136	-32.3393
b_i (J/mol·K^2)	1.8801	1.1365	1.8541
c_i (J/mol·K^3)	-0.0314	-0.0026	-0.00206
d_i (J/mol·K^4)	2.59×10^{-6}	2.43×10^{-6}	1.37×10^{-6}

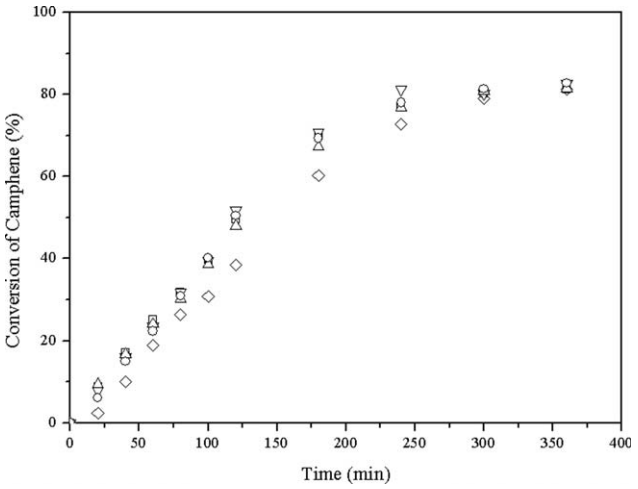

Figure 7. Effect of different agitation speed on the alkoxylation of camphene (temperature: 353 K; Lewatit2620 as catalyst; catalyst loading: 20% (w/w); molar ratio of camphene: MPO was 1:1, particle size: 0.5–0.62 mm) (◇) 200 rpm; (○) 300 rpm; (□) 400 rpm; (▽) 500 rpm; (△) 600 rpm.

Kinetics study

Influence of Mass Transfer. The influence of external diffusion could be eliminated by increasing the agitation speed. From Figure 7, it was concluded that with a stirring speed above 300 rpm there is no resistance because of external diffusion. Therefore, all further experiments were done at 400 rpm.

To evaluate the influence of the internal diffusion, Weisz–Prater criterion was used.[36] Thiele modulus is defined as Eq. 12

$$\varphi = \frac{r_p^2 k}{9D_e} \tag{12}$$

where r_p is the particle radius, k is observed reaction rate. D_e is the effective diffusion coefficient, φ is the Thiele modulus. When φ was smaller than 1, the internal diffusion could be neglected.

The effective diffusion coefficient was calculated by Eq. 13

Table 5. Parameters for LHHW Model for the Alkoxylation of Camphene with MPO

Apparent rate constant (mol/g min)	$k_f = 2.63\times10^5 \exp\left(-\frac{3504.47}{T}\right)$
Camphene adsorption	$K_C = 0.62\times\exp\left(\frac{896.75}{T}\right)$
MPO adsorption	$K_M = 2.79\times\exp\left(\frac{1505.35}{T}\right)$
IHIE adsorption	$K_I = 209.27\times\exp\left(-\frac{1160.65}{T}\right)$

$$D_e = \frac{\varepsilon_p D_A}{\tau} = \varepsilon_p^2 D_A \tag{13}$$

where τ is the tortuosity factor of the particle. ε_p is the particle porosity. D_A is the molecular diffusivity at infinite dilution calculated by the Wilke–Chang equation[34]

$$D_A = 7.4\times10^{-8}\frac{(\phi M)^{1/2}T}{\mu V_b^{0.6}} \tag{14}$$

where μ is the viscosity of the mixture, V_b is the molar volume at boiling point, which can be estimated by the Le Bas method.[34] ϕ is the associated factor. M is the molar mass of the component.

The values of Thiele modulus at 333–363 K were found to be 6.6×10^{-5}, 1.0×10^{-4}, 2.2×10^{-4}, 4.0×10^{-4}, respectively. All of them were smaller than 1, which indicating the internal diffusion could be neglected at 333–363 K.

Kinetic Model. Reactions catalyzed by cation exchange resin have been described by pseudohomogeneous (PH),[21,37,38] Eley–Rideal (ER),[13,37] and LHHW[21,37,39] models. In this study, all of the components were assumed to be absorbed on the surface of catalysts, a LHHW mechanism was developed and the following steps were considered

Camphene/MPO adsorption: $\mathrm{cam}+\mathrm{S}\overset{K_C}{\rightleftharpoons}\mathrm{cam}\cdot\mathrm{S}$

$$\mathrm{MPO}+\mathrm{S}\overset{K_M}{\rightleftharpoons}\mathrm{MPO}\cdot\mathrm{S}$$

Surface reaction: $\mathrm{cam}\cdot\mathrm{S}+\mathrm{MPO}\cdot\mathrm{S}\overset{k_f}{\rightleftharpoons}\mathrm{IHIE}\cdot\mathrm{S}+\mathrm{S}$

IHIE desorption: $\mathrm{IHIE}\cdot\mathrm{S}\overset{K_I}{\rightleftharpoons}\mathrm{IHIE}+\mathrm{S}$

Assuming the surface reaction between absorbed camphene and absorbed MPO was the rate-controlling step and the other steps reached equilibrium, the reaction rate for LHHW model based on activity can be written as follows

$$r = \frac{M_{cat}k_f\left(a_{cam}a_{MPO} - \frac{1}{K}a_{IHIE}\right)}{\left(1+K_C a_{cam}+K_M a_{MPO}+K_I a_{IHIE}\right)^2} \tag{15}$$

The temperature dependence of the estimated parameters can be described by the Arrhenius law

$$k_f = k_0\ \exp\left(-\frac{E}{RT}\right) \tag{16}$$

$$K_i = K_{0,i}\ \exp\left(-\frac{\Delta H_i}{RT}\right) \tag{17}$$

where M_{cat} is the catalyst mass per unit volume of the reactants, k_f is apparent rate constant, K_C, K_M, and K_I represent equilibrium adsorption constant of camphene, MPO, and IHIE, respectively. k_0 is pre-exponential factor for the reaction, E is activation energy, ΔH_C, ΔH_M, and ΔH_I represent adsorption enthalpy of camphene, MPO, and IHIE, respectively. $K_{0,C}$, $K_{0,M}$, and $K_{0,I}$ represent coefficient for K_C, K_M, and K_I in Eq. 17, respectively.

The equation coming from introducing the rate equation (Eq. 15) into the material balance from camphene was integrated by a fourth-order Runge–Kutta method. The parameters for the kinetic model are estimated by minimizing of the sum of residual squares (SRS) between the conversion of camphene through experiments and that calculated from kinetic model. Mathematically, this can be written as Eq. 18

$$\mathrm{SRS} = \sum\left(x_{exp} - x_{cal}\right)^2 \tag{18}$$

The nonlinear least-squares method was used for optimization. Parameters for the LHHW model were presented in Table 5. The activation energy was found to be 29.14 kJ/mol. From Figure 8, the values calculated from LHHW model were in good agreement with the experimental ones, which indicating that LHHW model gave a good representation of alkoxylation of camphene with MPO.

Comparison between different reactors

Based on the optimum conditions for the alkoxylation of camphene with MPO, the experiments were carried out in a 5-L double layer glass reaction kettle. The reactions in two different reactors with different capacities were compared at the camphene:MPO molar ratio of 1:1, reaction temperature of 353 K, and catalyst loading of 20% (w/w). Both the conversion of camphene and the yield of IHIE were similar (Figure 9), suggesting that the catalytic reaction was highly repeatable and reproducible. With the reaction conditions and kinetic parameters optimized, it is industrially feasible to alkoxylate camphene with MPO under the catalysis of Lewatit2620 to produce IHIE.

Conclusion

The conditions for the alkoxylation of camphene with MPO over Lewatit2620 were optimized as follows: initial molar ratio of MPO to camphene, 1:1; catalyst loading based on the total mass of reactants, 20%; reaction temperature, 353 K; and reaction time, 4 h. Under the optimum conditions, the conversion was 78.80% and the selectivity was

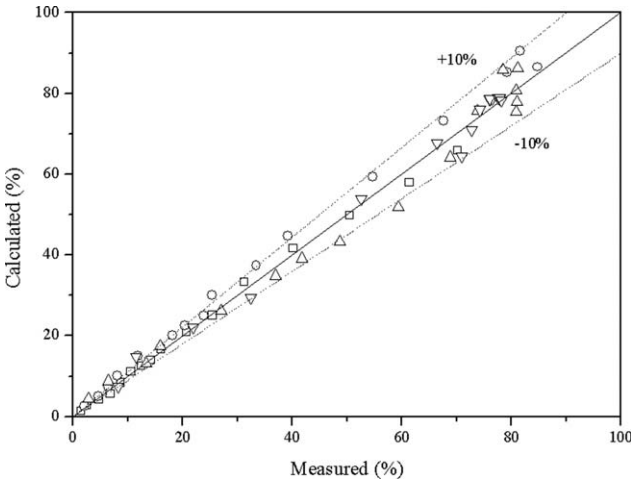

Figure 8. Comparison between measured and calculated conversions of camphene at different temperatures (□) 333 K; (○) 343 K; (△) 353 K; (▽) 363 K.

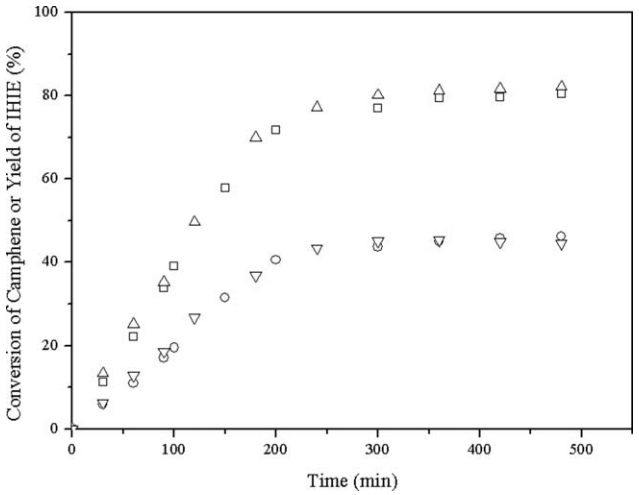

Figure 9. Comparison between different-sized reactions on the alkoxylation of camphene (temperature: 353 K; Lewatit2620 as catalyst; catalyst loading: 20% (w/w); molar ratio of camphene: MPO was 1:1).

Conversion of camphene: (□) 5 L; (△) 25 mL; Yield of IHIE: (○) 5 L; (▽) 25 mL.

93.5%. Besides, the catalyst was satisfactorily reusable. When treated as a function of temperature, the enthalpy change of reaction (-74.6 ± 3.3 kJ/mol) was closer to that calculated by Gaussian software (-75.73 kJ/mol) than that when treated as constant (-30.2 ± 1.2 kJ/mol). A LHHW kinetic model was used to correlate the experimental data and the activation energy was found to be 29.14 kJ/mol. Notably, the outcomes of large-scale experiments (5 L) resembled those of small-scale ones (250 mL).

Acknowledgment

Financial support for this work from National Natural Science Foundation of China (No. 21306078 and No. 21476105) and Natural Science Foundation of Jiangsu Province (No. BK2011633) is gratefully acknowledged.

Notation

a_{cam} = activity of camphene in the liquid phase, mol/L
a_{IHIE} = activity of isobornyl hydroxyl isobutyl ether in the liquid phase, mol/L
a_{MPO} = activity of 2-methyl-1,3-propanediol in the liquid phase, mol/L
$C_{p,i}$ = molar heat capacity of the component, J/mol·K
D_A = infinite dilution molecular diffusivity, cm^2/s
D_e = effective diffusion coefficient of component j inside the particle, cm^2/s
E = activation energy, kJ/mol
K = equilibrium constant of the reaction
k_f = apparent rate constant, mol/g·min
K_C = equilibrium adsorption constant of camphene
K_I = equilibrium adsorption constant of IHIE
K_M = equilibrium adsorption constant of MPO
k = observed reaction rate, mol/g min
k_0 = pre-exponential factor for the reaction, mol/g·min
$K_{0,C}$ = coefficient for K_C in Eq. 17, mol/g·min
$K_{0,I}$ = coefficient for K_I in Eq. 17, mol/g·min
$K_{0,M}$ = coefficient for K_M in Eq. 17, mol/g·min
M = molar mass, mol/L
M_{cat} = catalyst mass per unit volume of the reactants, g/L
r_p = particle radius, mm
R = gas constant, J/mol·K
t = time, min
T = temperature, K
w/w = weight of catalyst/weight of total reactants
V = volume of the reactants, cm^3
V_b = molar volume at the boiling point, cm^3/mol
x_{cal} = calculated conversion
x_{exp} = experimental conversion
ϕ = associated factor
μ = viscosity of the mixture, mPa·s
ε_p = particle porosity
τ = the tortuosity factor of the particle
$\Delta_r G^0$ = Gibbs free energy, kJ/mol
$\Delta_r H^0$ = reaction enthalpy, kJ/mol
$\Delta_r S^0$ = entropy, J/mol·K
ΔH_C = adsorption enthalpy of camphene, kJ/mol
ΔH_I = adsorption enthalpy of IHIE, kJ/mol
ΔH_M = adsorption enthalpy of MPO, kJ/mol

List of abbreviations

cam = camphene
IHIE = isobornyl hydroxyl isobutyl ether
MPO = 2-methyl-1,3-propanediol
ER = Eley–Rideal model
LHHW = Langmuir–Hinshelwood–Hougen–Watson model
PH = pseudohomogeneous model
SRS = residual squares

Literature Cited

1. Mateo JJ, Jiménez M. Monoterpenes in grape juice and wines. *J Chromatogr A*. 2000;881:557–567.
2. Crowell PL. Monoterpenes in breast cancer chemoprevention. *Breast Cancer Res Treat*. 1997;46:191–197.
3. Rozenbaum HF, Patitucci ML, Antunes OAC, Pereira N Jr. Production of aromas and fragrances through microbial oxidation of monoterpenes. *Braz J Chem Eng*. 2006;23:273–279.
4. Gershenzon J, Dudareva N. The function of terpene natural products in the natural world. *Nat Chem Biol*. 2007;3:408–414.
5. Kare MR. Some functions of the sense of taste. *J Agric Food Chem*. 1969;17:677–680.
6. Scheidl F, Gscheidmeier M. Terpene ethers. US Patent US4,590,302 A. May 20, 1986.
7. Royals EE. Synthesis of terpinyl ethers from d-limonene. *J Am Chem Soc*. 1949;71:2568–2571.
8. Lin Z, Gu Y. The reaction of camphene with ethyl alcohol under microwave irradiation. *J Nanjing Forestry Univ*. 2001;25:21–24.
9. Pito DS, Matos I, Fonseca IM, Ramos AM, Vital J, Castanheiro JE. Methoxylation of α-pinene over heteropolyacids immobilized in silica. *Appl Catal A Gen*. 2010;373:140–146.
10. Caiado M, Machado A, Santos RN, Matos I, Fonseca IM, Ramos AM, Vital J, Valente AA, Castanheiro JE. Alkoxylation of camphene over silica-occluded tungstophosphoric acid. *Appl Catal A Gen*. 2013;451:36–42.
11. Hensen K, Mahaim C, Hölderich WF. Alkoxylation of limonene and alpha-pinene over beta zeolite as heterogeneous catalyst. *Appl Catal A Gen*. 1997;149:311–329.
12. Yang G, Liu Y, Zhou Z, Zhang Z. Kinetic study of the direct hydration of turpentine. *Chem Eng J*. 2011;168:351–358.
13. Liu Y, Zhou Z, Yang G, Wu Y, Zhang Z. Kinetics study of direct hydration of dihydromyrcene in a jet reactor. *Ind Eng Chem Res*. 2010;49:3170–3175.
14. Liu Y, Zhou Z, Yang G, Zhang Z. Study on direct hydration of camphene to isoborneol by cation exchange resins. *Int J Chem React Eng A*. 2011;9:1–14.
15. Yadav GD, Thathagar MB. Esterification of maleic acid with ethanol over cation-exchange resin catalysts. *React Funct Polym*. 2002;52:99–110.
16. Komoń T, Niewiadomski P, Oracz P, Jamróz ME. Esterification of acrylic acid with 2-ethylhexan-1-ol: thermodynamic and kinetic study. *Appl Catal A Gen*. 2013;451:127–136.
17. Sharma M, Wanchoo R, Toor AP. Amberlyst 15 catalyzed esterification of nonanoic acid with 1-propanol: kinetics, modeling, and comparison of its reaction kinetics with lower alcohols. *Ind Eng Chem Res*. 2014;53:2167–2174.
18. Pereira CS, Pinho SP, Silva VM, Rodrigues AE. Thermodynamic equilibrium and reaction kinetics for the esterification of lactic acid with ethanol catalyzed by acid ion-exchange resin. *Ind Eng Chem Res*. 2008;47:1453–1463.

19. Guilera J, Bringué R, Ramírez E, Fité C, Tejero J. Kinetic study of ethyl octyl ether formation from ethanol and 1-octanol on Amberlyst 70. *AIChE J*. 2014;60:2918–2928.
20. Santacesaria E, Silvani R, Wilkinson P, Carra S. Alkylation of p-cresol with isobutene catalyzed by cation-exchange resins: a kinetic study. *Ind Eng Chem Res*. 1988;27:541–548.
21. Delgado P, Sanz MT, Beltrán S. Kinetic study for esterification of lactic acid with ethanol and hydrolysis of ethyl lactate using an ion-exchange resin catalyst. *Chem Eng J*. 2007;126:111–118.
22. Su CH, Fu CC, Gomes J, Chu I, Wu WT. A heterogeneous acid-catalyzed process for biodiesel production from enzyme hydrolyzed fatty acids. *AIChE J*. 2008;54:327–336.
23. Gandi GK, Silva VM, Rodrigues AE. Acetaldehyde dimethylacetal synthesis with Smopex 101 fibres as catalyst/adsorbent. *Chem Eng Sci*. 2007;62:907–918.
24. Silva VM, Rodrigues AE. Novel process for diethylacetal synthesis. *AIChE J*. 2005;51:2752–2768.
25. Gandi GK, Silva VM, Rodrigues AE. Process development for dimethylacetal synthesis: thermodynamics and reaction kinetics. *Ind Eng Chem Res*. 2005;44:7287–7297.
26. Graça NS, Pais LSS, Silva VM, Rodrigues AE. Oxygenated biofuels from butanol for diesel blends: synthesis of the acetal 1, 1-dibutoxyethane catalyzed by amberlyst-15 ion-exchange resin. *Ind Eng Chem Res*. 2010;49:6763–6771.
27. Radbil' AB, Kulikov MV, Sokolova TN, Kartashov VR, Zolin BA, Radbil' BA. Alkoxylation and hydration of camphene in the presence of acid catalysts. *Chem Nat Compd*. 1999;35:524–528.
28. Birladeanu L. The story of the Wagner-Meerwein rearrangement. *J Chem Educ*. 2000;77:858–863.
29. Li JJ. Wagner–Meerwein rearrangement. In: *Name Reactions*. Springer, 2009;566–567.
30. Buttersack C. Accessibility and catalytic activity of sulfonic acid ion-exchange resins in different solvents. *React Polym*. 1989;10:143–164.
31. Ancillotti F, Massi Mauri M, Pescarollo E, Romagnoni L. Mechanisms in the reaction between olefins and alcohols catalyzed by ion exchange resins. *J Mol Catal*. 1978;4:37–48.
32. Tejero J, Cunill F, Iborra M. Molecular mechanisms of MTBE synthesis on a sulphonic acid ion exchange resin. *J Mol Catal*. 1987;42:257–268.
33. Silva VM, Rodrigues AE. Kinetic studies in a batch reactor using ion exchange resin catalysts for oxygenates production: role of mass transfer mechanisms. *Chem Eng Sci*. 2006;61:316–331.
34. Dong X, Fang L, Chen L. *Principle to Estimate the Physical Properties and Computer Calculation*, 1st ed. Beijing: Chemical Industry Press, 2006.
35. Poling BE, Prausnitz JM, John Paul OC, Reid RC. *The Properties of Gases and Liquids*. New York: McGraw-Hill, 2001.
36. Weisz P, Hicks J. The behaviour of porous catalyst particles in view of internal mass and heat diffusion effects. *Chem Eng Sci*. 1962;17:265–275.
37. Gangadwala J, Mankar S, Mahajani S, Kienle A, Stein E. Esterification of acetic acid with butanol in the presence of ion-exchange resins as catalysts. *Ind Eng Chem Res*. 2003;42:2146–2155.
38. Yang G, Wu P, Zhou Z, He X, Meng W, Zhang Z. Direct hydration of β-caryophyllene. *Ind Eng Chem Res*. 2012;51:15864–15871.
39. Zhang Y, Ma L, Yang J. Kinetics of esterification of lactic acid with ethanol catalyzed by cation-exchange resins. *React Funct Polym*. 2004;61:101–114.

Manuscript received Dec. 29, 2014, and revision received Feb. 24, 2015.